Materials for Quantum Technology

PAPER

X-ray quantification of oxygen groups on diamond surfaces for quantum applications

N Dontschuk[1], LVH Rodgers[2], JP Chou[3], DA Evans[4], K M O'Donnell[5], HJ Johnson[1], A Tadich[6], AK Schenk[7], A Gali[8,9], NP de Leon[2] and A Stacey[1,10,11,*]

[1] School of Physics, University of Melbourne, Parkville, VIC 3010, Australia
[2] Department of Electrical and Computer Engineering, Princeton University, Princeton, NJ 08544, United States of America
[3] Department of Physics, National Changhua University of Education, Changhua, Taiwan
[4] Department of Physics, Aberystwyth University, Aberystwyth SY23 3BZ, United Kingdom
[5] Royal Melbourne Hospital, University of Melbourne, Parkville, Vic 3010, Australia
[6] Australian Synchrotron, 800 Blackburn Road, Clayton, Victoria 3168, Australia
[7] School of Computing, Engineering and Mathematical Sciences, La Trobe University, Bundoora, Victoria 3086, Australia
[8] Wigner Research Centre for Physics, POB 49, Budapest H-1525, Hungary
[9] Department of Atomic Physics, Budapest University of Technology and Economics, Műegyetem rakpart 3., Budapest H-1111, Hungary
[10] Princeton Plasma Physics Laboratory, 100 Stellarator Road, Princeton, NJ 08544, United States of America
[11] School of Science, RMIT University, Melbourne, VIC 3000, Australia
* Author to whom any correspondence should be addressed.

E-mail: astacey@pppl.gov

Keywords: oxygen terminated diamond, NEXAFS, XPS, surface spectroscopy, diamond surface for NV centres, DFT

Supplementary material for this article is available online

OPEN ACCESS

RECEIVED
16 June 2023

REVISED
21 August 2023

ACCEPTED FOR PUBLICATION
4 October 2023

PUBLISHED
30 October 2023

Abstract

Identifying the surface chemistry of diamond materials is increasingly important for device applications, especially quantum sensors. Oxygen-related termination species are widely used because they are naturally abundant, chemically stable, and compatible with stable nitrogen vacancy centres near the diamond surface. Diamond surfaces host a mixture of oxygen-related species, and the precise chemistry and relative coverage of different species can lead to dramatically different electronic properties, with direct consequences for near-surface quantum sensors. However, it is challenging to unambiguously identify the different groups or quantify the relative surface coverage. Here we show that a combination of x-ray absorption and photoelectron spectroscopies can be used to quantitatively identify the coverage of carbonyl functional groups on the {100} diamond surface. Using this method we reveal an unexpectedly high fraction of carbonyl groups (>9%) on a wide range of sample surfaces. Furthermore, through a combination of *ab initio* calculations and spectroscopic studies of engineered surfaces, we reveal unexpected complexities in the x-ray spectroscopy of oxygen terminated diamond surfaces. Of particular note, we find the binding energies of carbonyl-related groups on diamond differs significantly from other organic systems, likely resulting in previous misestimation of carbonyl fractions on diamond surfaces.

Controlling and understanding diamond surfaces is crucial for quantum technologies based on diamond. For example, nanoscale sensing relies on placing nitrogen-vacancy (NV) centres close to the diamond surface to achieve high sensitivity and high spatial resolution [1, 2]; however charge traps and impurities can lead to magnetic and electric field noise, as well as charge instability of near-surface NV centres [3, 4]. Most NV centre experiments to date have utilized oxygen terminated surfaces because such surfaces occur naturally, are chemically stable, and are generally compatible with charge-stable and coherent shallow NV centres [3, 5]. However, oxygen terminated diamond surfaces host a mix of groups including ether, carbonyl, hydroxyl, and residual hydrogen, and the specific chemical make up of surfaces has been shown to impact shallow NV properties [3, 6]. Even the 'best' oxygen terminations still exhibit substantial deleterious surface noise [4]. A key challenge for further optimization of quantum sensors is to properly characterize the coverage and structure of oxygen-related chemical species on single crystal diamond samples.

Understanding the chemical composition of single-crystal surface terminations is challenging because many chemical analysis tools are not sensitive enough to quantitatively analyse atomic monolayers. Instead, techniques such as soft x-ray photoelectron spectroscopy (XPS) must be used because the inelastic mean free path of photoelectrons guarantees that the detected signal originates from the top few nanometres of material. To date, the complexity of carbon—oxygen bonding has frustrated quantitative analysis using these approaches. XPS exhibits multiple overlapping components in both oxygen and carbon core levels without clear spectral identification of the associated chemical species. X-ray absorption, such as near edge x-ray absorption fine structure spectroscopy (NEXAFS) also contains rich information about the surface species in diamond [7–9]. However, in the carbon k-edge spectrum the locations of known oxygen related resonances overlap with other common features [7]. Similarly, the oxygen k-edge spectrum contains fingerprint information that correlates with quantum device properties [3], however to date the associated resonances are not conclusively linked to the surface atomic structure [10–12], and the transition matrix elements associated with the absorption dipoles of each species are not quantitatively known. This frustrates quantification of the abundance of different surface species even in instances where qualitative identification is possible.

In this work we use a multimodal approach; we jointly analyse surface sensitive, synchrotron x-ray photo-electron and absorption spectroscopic data along with density functional theory (DFT) calculations to identify spectral features associated with 'pure' (hydrogen free) ether and carbonyl surfaces, created artificially under ultra-high vacuum (UHV) conditions. Because there is no hydrogen on these surfaces and therefore no alcohol groups, we can quantitatively interpret all our spectra as combinations of only ether and carbonyl species. This allows us to isolate separate spectroscopic fingerprints of ether and carbonyl surface groups and then quantify surface coverage of these species. The positive identification of carbonyl groups alone is of particular consequence for quantum devices, because such groups are known to introduce a low-lying unoccupied electron (acceptor) state and are a prime suspect for driving both surface Fermi pinning and magnetic noise at microelectronic and quantum device surfaces [3, 4, 9, 13, 14]. Further study of NV-containing diamond surfaces using this technique should allow for a more accurate estimation of surface electronic traps. This opens the door to quantitative assessment of electron trap densities and the development of quantitative decoherence models informed by that characterization.

1. Methods

1.1. Preparation of the diamond substrate

The sample was prepared by growing a $\sim$10 μm single crystal lightly boron doped diamond overlayer (approximately 100 Torr, gas flows of 300 sccm H_2, 2.5 sccm methane, 0.15 sccm of a 2% mixture of trimethylborane in H_2, $\approx$900 W microwave power) on a single crystal diamond substrate (Element Six). The sample was then inserted into UHV within a few hours of growth where it remained for the duration of the experiments. The diamond was initially heated to 450 °C for 1 h to remove atmospheric contamination. Next the hydrogen was stripped by a series of flash anneals to high temperatures >900 °C, chamber pressures remained below 10^{-7} mbar. Successful removal was determined by the appearance of the characteristic surface reconstruction peak in the XPS C1s core level, see supplementary figure 3. Both the hydrogen termination, and subsequent bare surface showed the expected 2×1 LEED pattern and were confirmed to be oxygen free via XPS survey scans, see supplementary figure 10. Additionally in C k-edge NEXAFS we observed: a shifted carbon $\pi^\star$ resonance corresponding to the reactive π-bonds that terminate (reconstruct) the bare diamond surface, the disappearance of the C–H peak, and the absence of a significant peak indicating point-defect C = C sites (supplementary figure 3). Indicating the formation of a high-quality bare diamond surface.

1.2. Formation of a hydrogen-free oxygen termination

The bare surface was exposed to high purity (99.9999%) molecular oxygen gas at room temperature in six successive dosages, each approximately an order of magnitude larger than the last, ranging from 1 Langmuir to 10^5 L. Chamber pressures during the exposures ranged from 10^{-8} mbar to 10^{-6} mbar. After a cumulative dosage of 10^4 L (fifth dose) no further increase in O1s peak area was observed despite increasing to a cumulative $\approx 10^5$ L (sixth) dosage, suggesting no further termination was possible with this method. The sample was then successively annealed for an hour at 450 °C, 700 °C, 850 °C and 1050 °C after which >99% of the added oxygen had been removed. At each deposition and annealing step NEXAFS and XPS core levels were measured, the full data set is provided in supplementary figure 3.

1.3. XPS

C1s and O1s spectra were collected at the Australian Synchrotron. High resolution scans were done with a photon energy of 350 eV (except where 330 eV is noted) for C1s and 850 eV for O1s (except where 600 eV is noted), a pass energy of 5 eV and an energy step of 0.05 eV. The detector was at normal incidence to the sample surface, an angle of 55° was set between incoming x-ray illumination and detector. In these settings C1s (O1s) photo-electrons have ≈65 eV (320 eV) of kinetic energy and we estimate the surface selectivity the measured signal originates from within the top ≈5 nm (≈10 nm) [15]. All diamond samples were sufficiently boron doped (≈100 ppm) to avoid any charging effects.

1.4. NEXAFS

O k-edge and C k-edge spectra where collected at the Australian Synchrotron, in tandem with XPS measurements. All measurements were done in partial electron yield mode using a channeltron detector and a microchannel plate detector. During all measurements 50% of the x-ray beam intensity (I_0) was monitored on wire grid with another 10% of the beam hitting a reference foil. The pre-edge region of C k-edge spectra were taken with 0.05 eV energy step whilst the rest and O k-edge spectra were taken with 0.1 eV energy step. O k-edge spectra are normalised by I_0 with the post edge intensity (560 eV) being set to 1. C k-edge spectra are double normalised, first to I_0 and then to a photodiode measurement of x-ray intensity taken just past the normal sample position to account for carbon adsorption of the x-ray beam on the I_0 grid, the post edge intensity (320 eV) being set to 1. Energy referencing is done via fitting a characteristic peak on the associated reference foil, which has previously been referenced to the Au 4f line by the beamline scientists.

1.5. XPS fitting

Peak fitting was done using CasaXPS software [16], the 'LF' Voigt-like lineshape was used exclusively and was set to always be symmetric. All fit components are tabulated in supplementary tables I, II and III. Backgrounds were accounted for by a two step process, where a linear extrapolation from low binding energy was used to remove contributions from the secondary electron tail before a Shirley step background was applied. C1s background removal for the hydrogen-free oxygen termination is discussed in the main text. All spectra were referenced to the Au 4f line at 84 eV. All chemical shifts were calculated relative to the bulk diamond peak. All high resolution C1s and O1s spectra from the hydrogen free sample were intensity normalised to the low binding energy C1s tail to remove minor focus variations. Total peak areas were taken as the sum of all fit component areas.

1.6. NEXAFS component extraction with NMFF

Non-negative matrix factorisation (NMF) component extraction was implemented with the scikit-learn Python library [17], using a separate NMF model set for each illumination angle. The model was trained and fit on the set of O k-edge spectra from all oxygen depositions and annealing steps. Prior to fitting, the spectra were normalised and then smoothed with a three point running average filter. Initial component guesses were random, and the random seed was varied to maximise the separation of the $\pi^\star$ resonance between the two components.

1.7. DFT model of NEXAFS

A (4×4) in plane periodically repeating slab 5 layers thick of diamond {100}, was used to model the NEXAFS spectra from carbonyl components, shown in supplementary figure 8. Structure relaxations were first done using FHI-aims code [18] with a Perdew–Burke–Ernzerhof (PBE) exchange–correlation, a tight atom basis set and a $2 \times 2 \times 1$ Monkhorst–Pack k-point grid. Energies were calculated from this structure using the Quantum Espresso package [19], making use of XSpectra codes [20, 21]. The reference ground state energy was calculated using a standard self-consistent field (SCF), followed by a separate SCF calculation for the modified 'transition potential' at the absorber site (oxygen atom), then a set of unoccupied spectra are calculated for various photon polarization directions, using XSpectra code. Finally, transition energies are computed using a final calculation with a full electron removed from the core level of interest. These can be added in linear combinations to produce simulated NEXAFS spectra for arbitrary polarization angles, as plotted in figure 2(c). Further details of this approach can be found in previous publications [22].

1.8. DFT model of XPS

We considered the terrace of oxygenated {100} diamond surface by a supercell model with atomically smooth surface for the sake of simplicity. To this end, we used a slab model of {100} diamond where the top layer of the diamond surface was saturated by different variations of carbonyl, carboxyl, C–H and C–OH groups with ether chain connecting the two last groups. This procedure allows us to consider the effect on

the C1s and O1s peaks of the given surface terminator species in the presence of proximate surface terminator groups which may considerably broaden the respective XPS spectra.

The XPS peak of the selected atom was calculated by plane wave supercell DFT calculations as implemented in the VASP package [23, 24], using standard projector augmented wave projectors for carbon, oxygen, and hydrogen. We employed PBE functional [25] for the electronic structure calculations with Γ-point approximation which suffices for the 6×6 supercell of the surface. All the atoms were allowed to relax during the geometry optimization procedure, except for the carbon atoms at the bottom layer and the terminator groups of the previously constructed model. The quantum mechanical force threshold was set to 0.01 eV $Å^{-1}$.

To obtain an accurate surface core level shifts for comparison with experimental observations, we employed the Slater–Janak transition state approach within the final state approximation which is implemented in VASP [26–28]. We created four models with different surface oxygenated configurations. The initial slab model was constructed as described in [29], and had eighteen HO–COC–H terminators. We modified the initial model to build up three additional models with different surface terminations. These models, supplementary figure 7, were composed of twelve HO–COC–H with three HO–COCOCOC–H, fourteen HO–COC–H with six C = O, and fourteen HO–COC–H with four O = C–OH, respectively.

As the absolute energies from these calculations are not sufficiently accurate for direct comparison with the experimental data we used the following strategy for C1s and O1s core level shifts. For C1s spectra, we first picked up one carbon atom farthest from the bottom and top layers, and calculated the C1s XPS peak. Then the calculated level was shifted to the experimentally known sp^3 C1s peak, and we applied the same shift for each C1s peak as obtained for the atoms at the surface.

1.9. Oxygen termination preparations

Typical oxygen terminations were prepared via various combinations of common treatments, listed in supplementary table IV. The procedures used are as follows. Bristol boil: 30 min in boiling sulfuric acid with 8%w/v sodium nitrate. Tri-acid boil: 1 h in a refluxing 1 1:1 mixture of concentrated sulfuric, nitric, and perchloric acids. Piranha etch: 30 min 1:1 sulfuric acid and hydrogen peroxide at 90°C. O_2 Burn: Diamond annealed at 450 °C for 4 h in flowing O2 gas (purity 99.9999). Air burn: 450 °C for 1 h in air.

Of particular interest is the Princeton termination method, detailed in literature [3], as it produced the lowest measured fraction of carbonyl species. The diamond is prepared by mechanical polishing to a very flat surface (Ra < 100 pm roughness), reactive ion etching and a 1200°C relaxation anneal prior to nitrogen implantation. Post implantation NV is formed with 950°C vacuum anneal (10^{-6} mbar), the surface is prepared with a Bristol boil, tri-acid boil, Piranha etch, O_2 Burn and finally another Piranha etch. A simplified version of this process was also trialed, involving just acid boiling, O_2 burning and Piranha acid treatment, resulting in a comparable carbonyl fraction.

1.10. Oxygen coverage estimation

Oxygen coverage is estimated by comparing the measured ratio of O1s and C1s peak areas to the an expected ratio R_{SB} for 1 oxygen atom for each surface carbon atom, which we define as full monolayer coverage. R_{SB} is calculated as an overlayer thickness, with thickness $t = a_0/4$ a quarter of the atomic inter-layer spacing of diamond, using [15]:

$$R_{SB} = S * \frac{\left(1 - e^{-t/L_{TH}(E_{K,O})}\right)}{e^{-t/L_{TH}(E_{K,C})}} \tag{1}$$

$$S = \frac{F(\gamma_O)}{F(\gamma_C)} \frac{\sigma_O(\gamma_O)}{\sigma_C(\gamma_C)} \frac{T(E_{K,O})}{T(E_{K,C})} \frac{L_{QA}(E_{K,O})}{L_{QA}(E_{K,C})} \tag{2}$$

where γ is the illuminating x-ray photon energy and E_K is the kinetic energy of the emitted carbon (C) and oxygen (O) 1 s photoelectrons, F is the x-ray flux, σ is the theoretical photoionization cross section [30] and $T = \sqrt{(E_K)}/E_{\text{pass}}$ is the detector transmission function normalised by the set pass energy. L_{QA} and L_{TH} are the relevant predictive effective attenuation lengths for linearly polarised x-rays as described in [31]:

$$L_{TH} = \lambda_i (1 - 0.836\omega) \tag{3}$$

$$L_{QA} = \lambda_i \left(1 - 0.147\omega - 0.164\omega^2\right) \tag{4}$$

where $\omega(E_K)$ is the albeido and $\lambda_i(E_K)$ is the inelastic mean free path theoretically determined for diamond and taken from published values [31, 32].

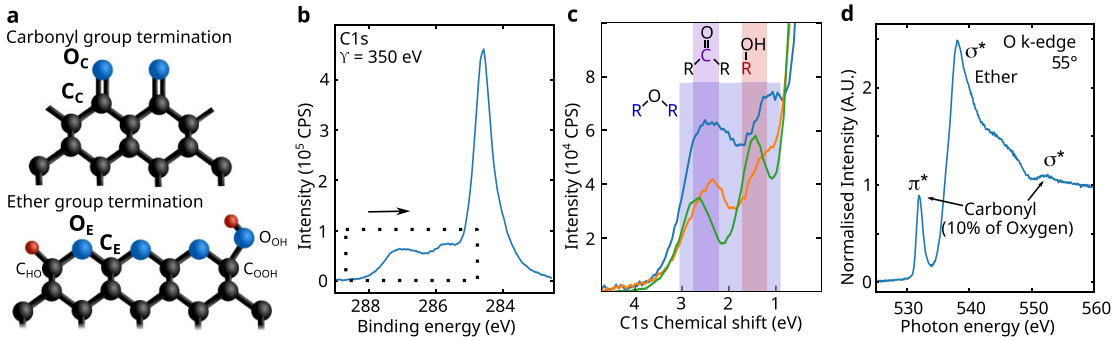

Figure 1. (a) Ball and stick cartoon of carbonyl and ether oxygen group terminations of a {100} diamond surface. Gray spheres indicate carbon, blue spheres are oxygen, and red spheres are hydrogen. (b) C1s XPS spectrum for a sample terminated with the Princeton method. Dashed box indicates high binding energy region. (c) High binding energy C1s XPS spectra for samples terminated with Princeton method (blue), ozone (green), and vacuum annealing (orange). Typical peak identities from molecules are indicated by shaded regions (see text). (D) O k-edge NEXAFS spectra for oxygen terminated diamond prepared by Princeton method with proposed component identities indicated with arrows.

2. Results

To understand the complexity of typical oxygen terminated diamond surfaces, one must consider the range of possible surface termination groups. In an artificially simple case, such as our experiment using high quality {100} diamond surfaces in UHV, a chemically pure oxygen terminated {100} diamond surfaces can contain only two oxygen groups (figure 1(a)): the ether group (C_E), where one oxygen is bonded to two surface carbon atoms, and the carbonyl group (C_C), where one oxygen is double-bonded to a single surface carbon [13, 14]. In a slightly more complex scenario, involving the ubiquitous prevalence of hydrogen in atmospherically stable oxygen terminations hydroxyl and hydrogen terminating groups must be considered. In terms of a majority ether-terminated {100} surface, ether chains can be terminated either by alcohol groups ($C_{O\,OH}$), or residual hydrogen ($C_{H\,O}$). These hydrogen-containing groups both increase the number of possible functional groups, confounding analysis with surface science techniques that cannot directly detect hydrogen [7, 14, 33–36].

As an example of such a surface, figure 1(b) shows a high resolution C1s XPS of a diamond terminated via the Princeton method [3], developed to improve near-surface quantum decoherence. Using standard XPS analysis approaches, the two resolvable chemical shift peaks to high binding energy of the C1s bulk diamond line would be assigned as surface carbon bonded to a single oxygen (285.7 eV), such as $C_{H\,O}$, and to two oxygen atoms (287 eV) as in C_E, C_C and $C_{O\,OH}$ [37]. Figure 1(c) shows a zoom in of these chemical shift components for this spectrum (blue line) compared to oxygen terminated diamonds prepared via ozone treatment (orange) and after high temperature vacuum annealing followed by acid cleaning (green). The shaded regions represent the chemical shifts observed from ether, ketone and alcohol molecules for comparison [14, 34, 38–41]. Even though individually each spectra shows two resolvable peaks, considered together it is clear that more than two (unresolvable) components make up the observed signal. As a result, it is not currently possible to reliably deconvolute C1s chemical shift data to determine the precise chemical make up of oxygen terminated diamond. We find that chemical shifts in high resolution O1s are similarly ambiguous (see supplementary figure 1). X-ray absorption spectroscopy provides an independent fingerprinting avenue. However, it is also known that the carbon k-edge NEXAFS peaks associated with oxygen overlap with other carbon features [7] near the 'bright line' absorption edge. The oxygen k-edge spectra from such diamonds should provide an ideal fingerprinting opportunity for revealing oxygen-specific chemistry. However, oxygen k-edge NEXAFS is not well studied on diamond. One particular spectral feature, as revealed on diamonds also terminated with the Princeton method (figure 1(c)), is a clear pre-edge peak at 531 eV, typically assigned to carbonyl $\pi^\star$ orbitals, but with some contention [10–12]. This peak makes an ideal tool to begin the process of quantitative characterisation of oxygen terminations. It is well separated from the main absorption edge and its height is proportional to the fraction of carbonyl-bonded oxygen. To make quantitative use of this signature peak, and determine its related $\sigma^\star$ components, we need first to confirm it is related to carbonyl species and then determine a calibration factor relating the peak area with overall oxygen composition. This latter goal requires determining the relative adsorption cross section of the carbonyl resonance by calibrating measured peak heights with an absolute measure of oxygen species on a reference sample.

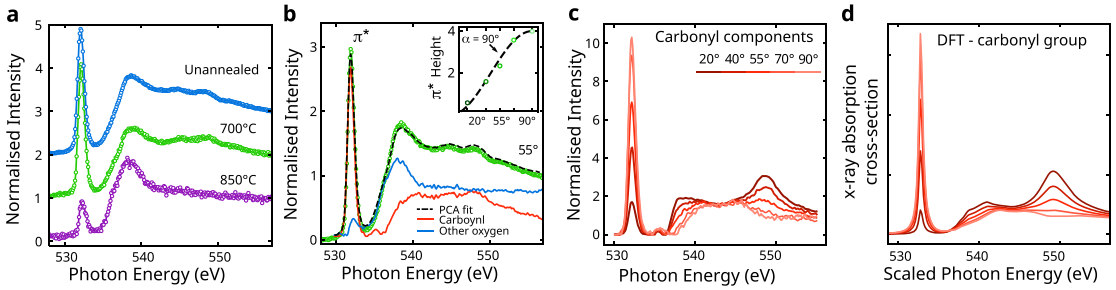

Figure 2. (a) NEXAFS O k-edge spectra of the saturated oxygen surface prepared by *in situ* annealing and oxygen exposure (blue), then subsequently annealed in vacuum at 700 °C (green) and 850 °C (purple). (b) Typical component deconvolution of O k-edge spectra from a hydrogen-free oxygen terminated diamond surface, all deconvolutions are shown in supplementary figure 2. Inset: $\pi^\star$ peak height as a function of NEXAFS illumination angle (green circles), fit with $\alpha = 90°$ π vector tilt angle formula [1]. (c) Angle resolved extracted carbonyl components. (d) DFT-derived simulations of bare surface with pure single carbonyl termination, scaled in energy to match experimental data in panel (c). There is excellent agreement between the simulated and experimentally extracted carbonyl spectra. Coloration legend as in panel (c).

Combined analysis with XPS, where peak intensities are more trivially related to fractional surface coverage, provides a convenient *in situ* method to perform this calibration. To overcome the aforementioned issues with deconvolution and create a reference sample, we prepared a set of simplified, hydrogen-free, oxygen terminations. This was done by first *in situ* thermally stripping the hydrogen from an oxygen-free as-grown hydrogen terminated sample. This bare diamond surface was then exposed to a source of clean molecular oxygen. After repeated exposures, the resulting surface was observed to saturate at around 0.5 monolayers, 1 oxygen atom for every 2 surface carbon atoms. The oxygen k-edge NEXAFS spectra of the saturated surface is shown in blue in figure 2(a). By comparison with figure 1(d) the set of clear features for this artificially generated surface are generally consistent with those observed on typical oxygen terminations, albeit with different component intensities.

In order to begin identifying features of this O k-edge NEXAFS spectrum, we examined the evolution of the spectrum over a series of *in situ*, 1 h-long anneals at increasing temperatures. During these heating experiments the different oxygen groups were expected to desorb at different temperatures. A 450 °C anneal resulted in no substantial changes seen in either XPS or NEXAFS spectra, as shown in supplementary figure 3. This resistance to moderate annealing is consistent with the oxygen being chemically bonded to the diamond. The 700 °C anneal resulted in removal of ≈60% of the oxygen, evidenced by reduction in O1s area (supplementary figure 4). At this temperature no significant preferential desorption of any particular species was observed (figure 2(a) green line). In contrast, an 850 °C temperature anneal (purple) resulted in a change of relative intensities of different features, specifically in the partial extinction of the $\pi^\star$ resonance and multiple post-edge features. Further extinction was observed after a final 1050 °C anneal, along with further decreases to the overall oxygen signal (supplementary figure 3). We understand this to be a result of preferential removal of carbonyl species. Remarkably, this is the only O k-edge spectra we have ever observed with such a small relative fraction of carbonyl (supplementary figure 5).

The angular evolution of the $\pi^\star$ resonance height, shown as the inset in figure 2(c), is consistent with the expected configuration of carbonyl oxygen bonded to a {100} diamond surface. This is characterised by a carbon–oxygen double bond normal to the diamond surface and a related planar dipole parallel with the surface (black dashed line) [42]. To further confirm this identification we recognise that the carbonyl-free surfaces produced with annealing allow us the opportunity to deconvolve the recorded NEXAFS spectra into two components and extract the spectral contribution of the carbonyl species itself. We approach this deconvolution using the NMF technique [17], and train it across every step in the aforementioned experiment. A typical extracted two component fit is shown in figure 2(b), with the carbonyl component shown in red and a composite of all other oxygen contributions shown in blue. This is repeated across all angles, as shown in supplementary figure 2, and the angular resolved extracted carbonyl spectrum is shown in figure 2(c). The observed strong variation of the resonance with angle is uncommon for oxygen terminated diamond, and is consistent with a high degree of regularity in the carbonyl orientation, with respect to the surface, as observed in highly smooth surfaces [3].

To confirm the assignment of this extracted spectra with carbonyl groups, we produced a simulation of isolated carbonyl on {100} diamond using DFT theory (figure 2(d)). The carbonyl group model consists of a single oxygen on a bare 2 × 1 reconstructed diamond slab, with the oxygen bonded as C = O occupying a broken C = C dimer (see section 1 for slab geometry). The simulation of the NEXAFS spectrum for oxygen on the structurally relaxed slab model followed the four step procedure in [22]. The

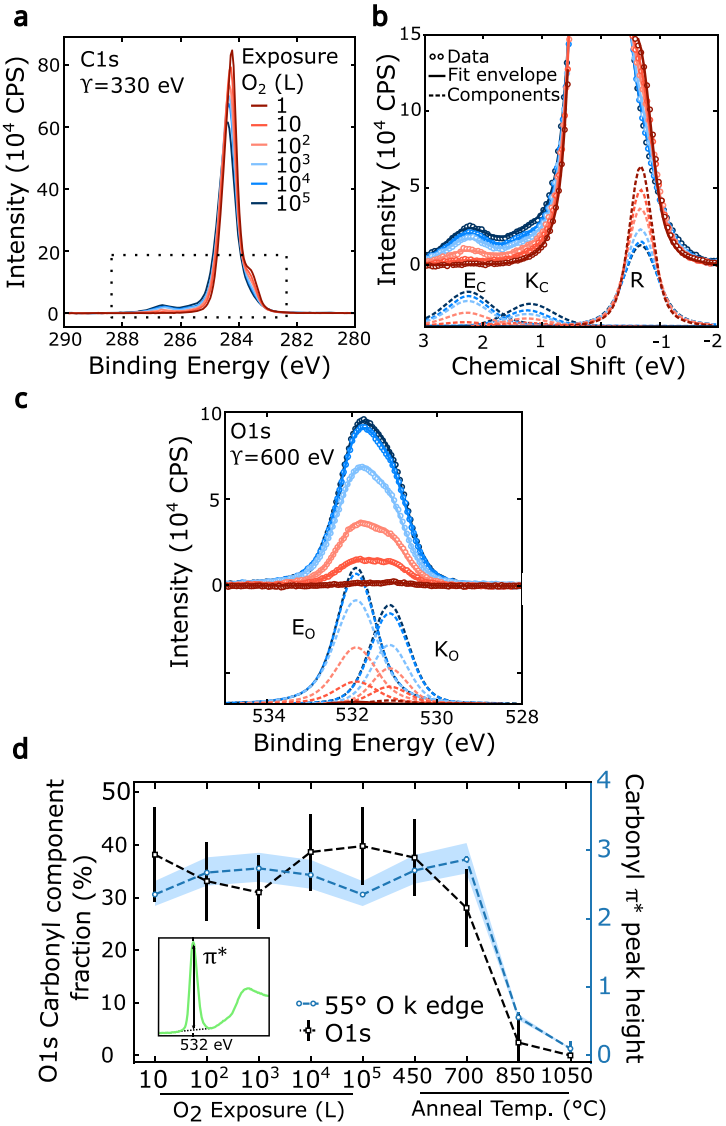

Figure 3. (a) C1s XPS scans of a reconstructed bare diamond surface exposed to successively larger doses of molecular oxygen. (b) Zoom-in of the C1s data, showing component fits for two oxygen-related groups, C_E and C_C, and the reconstruction component, R. (c) O1s XPS data with component fits O_E and O_C. The excitation photon energies are provided in (a) and (c). (d) Comparison of carbonyl fraction determined from O1s spectra and normalised NEXAFS O k-edge $\pi^\star$ peak height, with a 13× multiplier to convert $\pi^\star$ peak height to coverage. The blue shaded region represents the $\pm 1\times$ change in this factor.

extracted carbonyl component and the polarization dependence calculated by DFT (figure 2(d)) is a remarkable match to the experimentally extracted components. Three clear features are reproduced both theoretically and experimentally. These include the primary $\pi^\star$ peak and two other peaks near 550 eV and under the step edge below 540 eV. Both of these secondary peaks have angular dependences perpendicular to the $\pi^\star$ peak, consistent with $\sigma^\star$ features of the same carbonyl bonds. The only clear discrepancy is the small peak at 536 eV, seen in the NMF extracted carbonyl component, this peak sits under the step edge and is likely explained by inaccuracy in the component extraction. Taken together, these datasets allow us to convincingly associate the O k-edge $\pi^\star$ with carbonyl groups and begin the process of spectral decomposition for full chemical understanding of these surfaces.

We now revisit XPS peak assignments by examining corresponding C1s and O1s core level data collected for this same set of hydrogen-free oxygen terminations. The C1s spectra are shown in figures 3(a) and (b), for the full range of oxygen exposures up to the saturated oxygen coverage discussed previously. On the high binding energy side of the diamond bulk peak there are clear oxygen related components, but only one visually obvious peak. A shoulder (R) on the low binding energy side is indicative of the bare diamond surface [43]. To quantitatively analyse these spectra, we first produced a model for the background based on the bare diamond C1s spectrum, including a Shirley step-function to account for scattered photo-electrons and a polynomial background curve to account for the tail of secondary electrons (this is more prominent in

the surface sensitive mode we have used, see section 1). This multi-component background fits well with measurements from all oxygen coverages, and required only minor adjustment to ensure convergence at high binding energies (an example is provided in supplementary figure 6). The oxygen–carbon chemical shifts (relative to the diamond bulk peak position) were fit with just two components C_E and C_C, shown in figure 3(b). The two known diamond bulk components are not shown for clarity; full fits, lineshape details and fitting constraints can be found in supplementary figure 4 and supplementary table I. As expected, we observe a gradual increase in high binding energy components with increasing oxygen exposure. This is consistent with the formation of carbon–oxygen bonds, and a simultaneous reduction in the carbon–carbon π-bonding component (R), as the bare surface reconstruction reacts with the oxygen molecules. O1s spectra of these surfaces (figure 3(c)) show two clear oxygen components, labelled O_E and O_C. Similarly, we deconvolve these spectra by first creating a background model on the O1s spectra of the bare diamond surface, including the secondary electron background and Shirley step.

Comparison between the fitted O1s and C1s peaks show correlations, but between unexpected pairs. Typically, it is expected that a lower binding energy feature in O1s will correlate with a higher binding energy feature in C1s, based on an electron cloud density picture of the bonding and relative electronegativities of the component atoms. Instead, we observe the opposite: the low binding energy components C_C and O_C are correlated with each other, and are therefore assigned to the same physical oxygen group. By comparing changes in the oxygen peak ratios measured with XPS with the relevant O k-edge NEXAFS spectra, we can assign the C_C component to carbonyl oxygen which deviates from the position almost universally seen in XPS experiments of organic molecular samples. To quantify this comparison, figure 3(d) shows a scatter plot of the C_C component fraction against the normalised NEXAFS $\pi^\star$ peak height with an illumination angle of 55° to the sample surface (including baseline subtraction, as shown in the inset). These data include the full oxygen exposure and annealing sequence. The two sets agree within error when the normalised carbonyl $\pi^\star$ peak height is multiplied by approximately 13 ×. The blue shaded regions show the effect of varying this calibration factor between 12 × and 14 ×. This new calibration factor can be used to determine the fraction of carbonyl groups on a diamond surface from the normalised 55° O k-edge NEXAFS spectra alone. This also provides an estimate of the relative x-ray absorption cross section, which determines the normalised peak intensity of the O $\pi^\star$ resonance compared to the ionization tail at 555 eV. Scaling the measured normal-incidence $\pi^\star$ peak height (≈3.8) by the estimated carbonyl fraction (≈35%) estimates a normalised pure carbonyl resonance (≈11) that is consistent with the normalised extracted carbonyl components shown in figure 2(c).

3. Discussion

This outcome, derived from our artificially generated reference sample, is contingent on the unique assignment of the C_C C1s component in our data to carbonyl groups. To test the assumption of peak separability and identification here we investigate the peak assignment validity through DFT of the XPS binding energies. This was conducted by simulation of a mixed-oxygen and hydrogen surface model, where the terminated diamond surface is represented on 4 × 4 × 5 super cells with periodic boundary conditions, the terminations are varied and both hydrogen containing and hydrogen-free species are considered. Two such models are shown in figure 4(a), that contains a mixture of length 2 and length 4 ether chains, the other modelled surfaces are shown in supplementary figure 7. For each carbon and oxygen atom the expected 1 s binding energy was estimated and plotted in figure 4(b). To aid with visual comparison to experimental data the lower half shows an example of C1s and O1s core level spectra for the hydrogen-free termination, the position of common hydrogen containing group components are shown as dashed lines. The agreement in relative position of the carbonyl group component is compelling. This decrease in chemical shift of the carbonyl group compared to molecular assignment can be understood as a final state core-hole relaxation (de-localisation) and is predicted to also occur in other carbon allotropes [35], and the {110} diamond surface [44]. Given the discrepancy with molecular C1s chemical shifts, care must be taken in interpreting implicit and explicit estimations of the carbonyl fraction of oxygenated diamond surfaces using XPS [3, 34, 37, 45].

The multiple overlapping hydrogen containing components in C1s and O1s spectra and broad spread of calculated binding energies for each group, due to next-nearest neighbour interactions, provide a qualitative explanation for inconsistency seen in our data of typical surfaces and across literature in XPS component positions [14, 34, 36]. Of particular note is a marked overlap between C1s binding energies for terminal hydrogen ether chains and carbonyl groups, explaining our difficulty in deriving carbonyl fractions from C1s spectra alone.

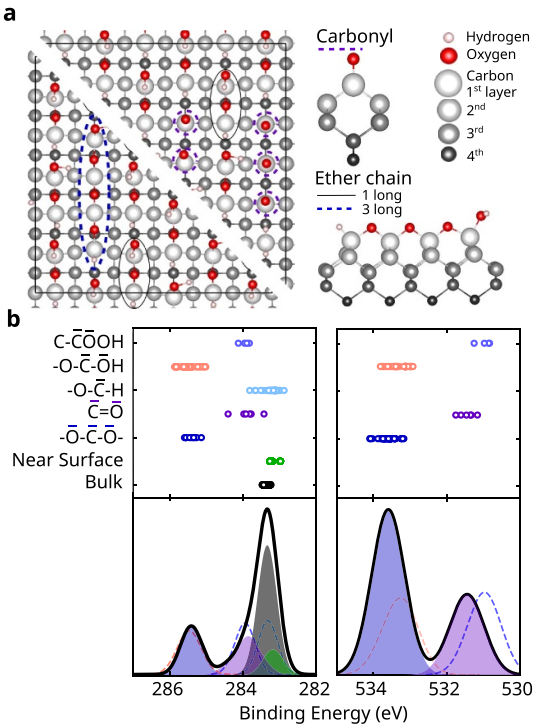

Figure 4. (a) Examples of two diamond slab surface configurations used to perform DFT simulations to extract C1s and O1s core level binding energies. Surface terminations considered included both oxygen and hydrogen species, the shown surfaces contain long ether chains (bottom left—blue dashed oval) and carbonyl groups (top right—purple dashed circles) (see sup. info. for full models). (b) (upper) The calculated binding energies for each atom plotted as open circles. (b) (lower) A visual representation of DFT-predicted XPS spectra for the hydrogen free surface, this is estimated by a sum of Gaussian lineshapes centred at each of the calculated binding energies (0.6 eV width) shown by the solid black line. Each individual chemical component is shown as shaded region. The combined peak area is arbitrary, and chosen to be similar to experimental data whilst having visible surface components. Hydrogen containing termination components are shown as dashed lines.

Armed with our above derived calibration factor we can now estimate the relative fraction of carbonyl groups (i.e. fraction of all surface oxygen species) in a way that is robust to the presence of hydrogen groups. We do this for a range of oxidised {100} single crystal diamond samples including mixtures of: boiling in acids, ozone exposure, oxygen plasma treatment, air burning and piranha solution treatment. Data analysis from 13 such samples (see supplementary figure 5) reveals a carbonyl fraction of between 9% ('Triacid boil') and 34% (atmospheric exposure of a bare surface), shown in figure 5. We note that the best sample surface, produced by the Princeton termination method, known to produce the shallowest NV centres with longest spin coherence time, has both lowest coverage of carbonyl and also highest total oxygen coverage. This approach to estimation of carbonyl fraction from O k-edge NEXAFS should extend trivially to other diamond surfaces, however experimental verification that the $\pi^\star$ relative x-ray adsorption cross section remains consistent across different diamond surfaces is required.

To test consistency with XPS the calculated carbonyl fractions were also used to constrain deconvolution of the O1s spectra of these real world samples into three components. The carbonyl component was fixed in position at 531 ± 0.5 eV, with its area set by the carbonyl fraction, see supplementary figure 9. Although not unique, the constrained fit agrees well with experimental data for all samples. Unfortunately, while the C1s simulations provide significant clarity, the number of overlapping components in C1s makes application of this library to C1s deconvolution uninformative for complex samples. A final consideration is that for most quantum sensing applications n-type doped diamond is required, however to obtain sufficient conductivity for high resolution XPS measurements we measure exclusively boron doped (p-type) diamond [46]. For multiple measured oxygen terminations, companion n-type diamonds underwent the same surface treatments and were measured in NEXAFS, which does not require conductive samples. As expected, differences in the bulk Fermi level had no observable effect on the chemical composition of surface termination.

In conclusion, we have demonstrated how multimodal x-ray photoelectron spectroscopies can be deployed for identifying and quantifying the oxygen-related termination chemistries on the {100} diamond

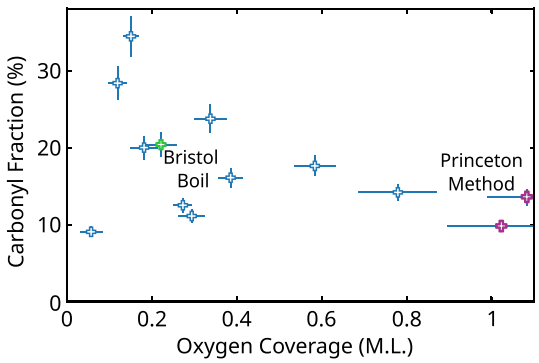

Figure 5. The carbonyl fraction estimated from NEXAFS vs oxygen coverage determined from O1s/C1s XPS peak area ratios for a range of typical oxygen surface preparations. Princeton method terminations are shown in purple, and a Bristol Boil termination is shown in green. Specific labels for the blue data points can be seen in supplementary figure 11 and associated surface treatments in supplementary table IV.

surface. Using a sequence of specially prepared pure-oxygen surfaces, we have combined x-ray photoelectron and absorption spectroscopies to quantify the fraction of carbonyl groups on the diamond surface and identify the unexpected binding energy of the C1s XPS component associated with carbonyl groups. Comparing this data with DFT-derived NEXAFS simulations we have confirmed that the NEXAFS absorption feature at 531 eV is indicative of a carbonyl $\pi^\star$ resonance, and measured the multiplication factor (13 ± 1) required to convert this resonance peak height into a quantitative measure of the fraction of oxygen groups in the carbonyl state on real surfaces. Further, we have presented a range of DFT-derived XPS simulations which confirm the unexpectedly low binding energy of carbonyl groups in diamond C1s spectra, and reveal a wide range of possible binding energies for other oxygen groups at the diamond surface. By using this analysis approach on a range of typical diamond surfaces, we have revealed a significant carbonyl fraction, often above 10% of the available surface sites. Since carbonyl groups are known to produce low lying unoccupied electronic states [34], this represents an unexpectedly high fraction of likely electron traps at the diamond surface, which are key candidates for electromagnetic noise sources and Fermi pinning at device surfaces. Finally we note that the presence of hydrogen groups on normal oxygen terminations makes XPS an unreliable tool for determining terminating species, and such analysis requires techniques that can better resolve hydrogen containing components such as FT-IR and HREELS [36].

Data availability statement

The data cannot be made publicly available upon publication because they are not available in a format that is sufficiently accessible or reusable by other researchers. The data that support the findings of this study are available upon reasonable request from the authors.

Acknowledgment

This material is based upon work supported by U.S. Department of Energy, Office of Science, Office of Fusion Energy Sciences and Office of Basic Energy Sciences under Award No. LAB 21-2491. Surface spectroscopy and analysis at Princeton was primarily supported by the US Department of Energy, Office of Science, Office of Basic Energy Sciences, under Award No. DE-SC0018978. Diamond surface preparation was supported by the NSF under the CAREER program (Grant DMR1752047). L V H R was supported by the National Defense Science and Engineering Graduate Fellowship. A G acknowledges the support from the NKFIH in Hungary for the National Excellence Program (Grant No. KKP129866), the Quantum Information National Laboratory (Grant No. 2022-2.1.1-NL-2022- 0000), and the EU QuantERA II MAESTRO project and from the European Commission for the QuMicro project (Grant No. 101046911). This research was undertaken on the Soft x-ray beam-line at the Australian Synchrotron, part of ANSTO. N D was support by an Australian Research Council Discovery Project Discovery Project (Grant 200103712). The United States Government retains a non-exclusive, paid-up, irrevocable, world-wide license to publish or reproduce the published form of this manuscript, or allow others to do so, for United States Government purposes.

Conflict of interest

The authors declare no conflicts of interest.

ORCID iDs

N Dontschuk https://orcid.org/0000-0001-6061-7537
JP Chou https://orcid.org/0000-0001-8336-6793
A Gali https://orcid.org/0000-0002-3339-5470

References

[1] Grinolds M S *et al* 2014 Subnanometre resolution in three-dimensional magnetic resonance imaging of individual dark spins *Nat. Nanotechnol.* **9** 279–84
[2] Sushkov A Lovchinsky I, Chisholm N, Walsworth R L, Park H and Lukin M D 2014 Magnetic resonance detection of individual proton spins using quantum reporters *Phys. Rev. Lett.* **113** 197601
[3] Sangtawesin S *et al* 2019 Origins of diamond surface noise probed by correlating single-spin measurements with surface spectroscopy *Phys. Rev.* X **9** 031052
[4] Dwyer B L *et al* 2022 Probing spin dynamics on diamond surfaces using a single quantum sensor *PRX Quantum* **3** 040328
[5] Yamano H *et al* 2017 Charge state stabilization of shallow nitrogen vacancy centers in diamond by oxygen surface modification *Jpn. J. Appl. Phys.* **56** 04CK08
[6] Henshaw J *et al* 2022 Nanoscale solid-state nuclear quadrupole resonance spectroscopy using depth-optimized nitrogen-vacancy ensembles in diamond *Appl. Phys. Lett.* **120** 174002
[7] Shpilman Z *et al* 2014 A near edge x-ray absorption fine structure study of oxidized single crystal and polycrystalline diamond surfaces *Diam. Relat. Mater.* **45** 20–27
[8] Bobrov K *et al* 2001 Surface electronic states of the partially hydrogenated diamond C(100)−(2 × 1) : H surface *Phys. Rev.* B **63** 165421
[9] Stacey A *et al* 2019 Evidence for primal sp^2 defects at the diamond surface: candidates for electron trapping and noise sources *Adv. Mater. Interfaces* **6** 1801449
[10] Gao X *et al* 2008 Water-induced negative electron affinity on diamond (100) *J. Phys. Chem.* C **112** 2487–91
[11] Reinke P, Knop-Gericke A, Hävecker M and Schedel-Niedrig T 2000 Interaction of diamond with water: an *in situ* XANES investigation *Surf. Sci.* **447** 229–36
[12] Baldwin C G, Downes J E, McMahon C J, Bradac C and Mildren R P 2014 Nanostructuring and oxidation of diamond by two-photon ultraviolet surface excitation: an XPS and NEXAFS study *Phys. Rev.* B **89** 195422
[13] Sque S J, Jones R and Briddon P R 2006 Structure, electronics and interaction of hydrogen and oxygen on diamond surfaces *Phys. Rev.* B **73** 085313
[14] Navas J *et al* 2018 Oxygen termination of homoepitaxial diamond surface by ozone and chemical methods: an experimental and theoretical perspective *Appl. Surf. Sci.* **433** 408–18
[15] Jablonski A 2019 Evaluation of procedures for overlayer thickness determination from XPS intensities *Surf. Sci.* **688** 14–24
[16] Fairley N *et al* 2021 Systematic and collaborative approach to problem solving using x-ray photoelectron spectroscopy *Appl. Surf. Sci. Adv.* **5** 100112
[17] Pedregosa F *et al* 2011 Scikit-learn: machine learning in python *J. Mach. Learn. Res.* **12** 2825–30
[18] Blum V *et al* 2009 *Ab initio* molecular simulations with numeric atom-centered orbitals *Comput. Phys. Commun.* **180** 2175–96
[19] Giannozzi P *et al* 2009 Quantum espresso: a modular and open-source software project for quantum simulations of materials *J. Phys.: Condens. Matter* **21** 395502
[20] Taillefumier M, Cabaret D, Flank A-M and Mauri F 2002 x-ray absorption near-edge structure calculations with the pseudopotentials: application to the k edge in diamond and α-quartz *Phys. Rev.* B **66** 195107
[21] Gougoussis C, Calandra M, Seitsonen A P and Mauri F 2009 First-principles calculations of x-ray absorption in a scheme based on ultrasoft pseudopotentials: from α-quartz to high-t_c compounds *Phys. Rev.* B **80** 075102
[22] O'Donnell K M *et al* 2016 Orientation and stability of a bi-functional aromatic organic molecular adsorbate on silicon *Phys. Chem. Chem. Phys.* **18** 27290–9
[23] Kresse G and Hafner J 1993 *Ab initio* molecular dynamics for liquid metals *Phys. Rev.* B **47** 558–61
[24] Kresse G and Furthmüller J 1996 Efficient iterative schemes for *ab initio* total-energy calculations using a plane-wave basis set *Phys. Rev.* B **54** 11169–86
[25] Perdew J P, Burke K and Ernzerhof M 1996 Generalized gradient approximation made simple *Phys. Rev. Lett.* **77** 3865
[26] Janak J F 1978 Proof that $\frac{\partial e}{\partial n_i} = \epsilon$ in density-functional theory *Phys. Rev.* B **18** 7165–8
[27] Lizzit S *et al* 2001 Surface core-level shifts of clean and oxygen-covered Ru(0001) *Phys. Rev.* B **63** 205419
[28] Köhler L and Kresse G 2004 Density functional study of CO on Rh(111) *Phys. Rev.* B **70** 165405
[29] Kaviani M *et al* 2014 Proper surface termination for luminescent near-surface NV centers in diamond *Nano Lett.* **14** 4772–7
[30] Yeh J J and Lindau I 1985 Atomic subshell photoionization cross sections and asymmetry parameters: 1 Z 103 *At. Data Nucl. Data Tables* **32** 1–155
[31] Jablonski A and Powell C J 2020 Effective attenuation lengths for different quantitative applications of x-ray photoelectron spectroscopy *J. Phys. Chem. Ref. Data* **49** 033102
[32] Tanuma S, Powell C J and Penn D R 2011 Calculations of electron inelastic mean free paths. IX. Data for 41 elemental solids over the 50 eV to 30 keV range *Surf. Interface Anal.* **43** 689–713
[33] Schenk A K *et al* 2016 High resolution core level spectroscopy of hydrogen-terminated (1 0 0) diamond *J. Phys.: Condens. Matter* **28** 305001
[34] Alba G, Villar M P, Alcántara R, Navas J and Araujo D 2020 Surface states of (100) O-terminated diamond: towards other 1 × 1:O reconstruction models *Nanomaterials* **10** 1193
[35] Aarva A, Deringer V L, Sainio S, Laurila T and Caro M A 2019 Understanding x-ray spectroscopy of carbonaceous materials by combining experiments, density functional theory and machine learning. part I: fingerprint spectra *Chem. Mater.* **31** 9243–55
[36] Li F, Akhvlediani R, Kuntumalla M and Hoffman A 2019 Oxygen bonding configurations and defects on differently oxidized diamond surfaces studied by high resolution electron energy loss spectroscopy and x-ray photoelectron spectroscopy measurements *Appl. Surf. Sci.* **465** 313–9
[37] Gengenbach T R, Major G H, Linford M R and Easton C D 2021 Practical guides for x-ray photoelectron spectroscopy (XPS): interpreting the carbon 1s spectrum *J. Vac. Sci. Technol.* A **39** 013204

[38] López G P, Castner D G and Ratner B D 1991 XPS O 1s binding energies for polymers containing hydroxyl, ether, ketone and ester groups *Surf. Interface Anal.* **17** 267–72
[39] Kitagawa F *et al* 2011 XPS and NEXAFS studies of VUV/O3-treated aromatic polyurea and its application to microchip electrophoresis *IET Nanobiotechnol.* **5** 136–42
[40] Kostov K dos Santos A L R, Honda R Y, Nascente P A P, Kayama M E, Algatti M A and Mota R P 2010 Treatment of PET and PU polymers by atmospheric pressure plasma generated in dielectric barrier discharge in air *Surf. Coat. Technol.* **204** 3064–8
[41] Zhang W Carravetta V, Plekan O, Feyer V, Richter R, Coreno M and Prince K C 2009 Electronic structure of aromatic amino acids studied by soft x-ray spectroscopy *J. Chem. Phys.* **131** 035103
[42] Stöhr J 1992 *Nexafs Spectroscopy* 1st edn (Springer)
[43] Schenk A Tadich A, Sear M, O'Donnell K M, Ley L, Stacey A and Pakes C 2015 Formation of a silicon terminated (100) diamond surface *Appl. Phys. Lett.* **106**, 191603
[44] Chaudhuri S *et al* 2022 Coexistence of carbonyl and ether groups on oxygen-terminated (110)-oriented diamond surfaces *Commun. Mater.* **3** 1–9
[45] Sulthana N M, Ganesan K, Ajikumar P and Dhara S 2022 Studies on tuning surface electronic properties of hydrogenated diamond by oxygen functionalization *Diam. Relat. Mater.* **128** 109284
[46] Astley S *et al* 2022 Identifying chemical and physical changes in wide-gap semiconductors using real-time and near ambient-pressure xps *Faraday Discuss.* **236** 191–204